Hydrogen Evolution Mediated by Cobalt Diimine-Dioxime Complexes: Insights into the Role of the Ligand Acid/Base Functionalities.

Dongyue Sun, Aparna Karippara Harshan, Jacques Pécaut, Sharon Hammes-Schiffer, Cyrille Costentin, Vincent Artero

Title: Hydrogen Evolution Mediated by Cobalt Diimine-Dioxime Complexes: Insights into the Role of the Ligand Acid/Base Functionalities.

Authors: Dongyue Sun; Arpana Karippara Harshan; Jacques Pécaut; Sharon Hammes-Schiffer; Cyrille Costentin; Vincent Artero

To be cited as: 10.1002/celc.202100413

Link to VoR: https://doi.org/10.1002/celc.202100413

Hydrogen Evolution Mediated by Cobalt Diimine-Dioxime Complexes: Insights into the Role of the Ligand Acid/Base Functionalities.

Dongyue Sun,[1] Arpana Karippara Harshan,[2] Jacques Pécaut,[3] Sharon Hammes-Schiffer,[4] Cyrille Costentin*[5,6] and Vincent Artero*[1]

[1] Dr D. Sun, Dr V. Artero

Univ. Grenoble Alpes, CNRS, CEA, IRIG, Laboratoire de Chimie et Biologie des Métaux, 17 rue des Martyrs, F-38054 Grenoble, Cedex, France; vincent.artero@cea.fr

[2] Dr A. Karippara Harshan

Department of Chemistry, Pennsylvania State University, University Park, Pennsylvania 16802 United States.

[3] Dr J. Pécaut

Univ. Grenoble Alpes, CNRS, CEA, IRIG, SyMMES, 17 rue des Martyrs, F-38054 Grenoble, Cedex, France.

[4] Prof. S. Hammes-Schiffer

Department of Chemistry, Yale University, New Haven, Connecticut 06520 United States.

[5] Prof. C. Costentin

Univ Grenoble Alpes, CNRS, DCM, 38000 Grenoble, France; cyrille.costentin@univ-grenoble-alpes.fr

[6] Prof. C. Costentin

Université de Paris, 75013 Paris, France.

To the memory of Prof. Jean-Michel Savéant

ABSTRACT

The benchmarking of the performance for H_2 evolution of cobalt diimine-dioxime catalysts is provided based on a comprehensive study of their catalytic mechanism. The latter follows an ECE'CC pathway with intermediate formation of a Co(II)-hydride intermediate and second protonation possibly at a basic site of the ligand, acting as a proton relay. This suggests an intramolecular coupling between the hydride and protonated ligand as the proton concentration-independent rate-determining step controlling the turnover frequency for H_2 evolution.

Graphical abstract

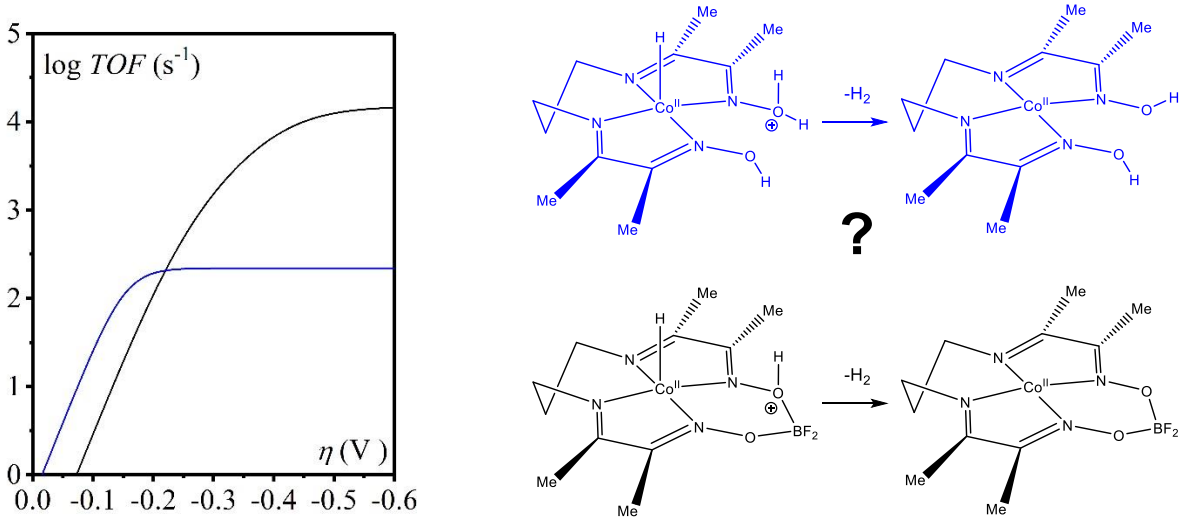

Table of Contents text:

Cobalt diimine-dioxime complexes are versatile catalysts for H_2 evolution but the benchmarking of their performances was still lacking. This article fills this gap based on the report of their catalytic response under canonical conditions allowing, thanks to a newly developed analytical treatment, a comprehensive description of the mechanism at play with a proton-independent rate-determining step. The authors also demonstrate that not every basic site installed in the second coordination sphere can act as proton relay in catalysis.

INTRODUCTION

Hydrogen as an energy carrier is a promising alternative to fossil fuels provided it is produced using renewable energy via electrolysis. A related key challenge is the finding of new efficient and robust catalysts based on Earth-abundant elements for the reduction of protons into H_2. Among molecular catalysts, bis-glyoximato cobalt complexes (cobaloximes) appear as one of the most active series when considering turnover frequencies and overpotential requirements.[1] Cobalt diimine-dioxime complexes (Figure 1) with a tetradentate equatorial ligand similarly displayed good performances in terms of overpotential requirements,[2] are even more stable against hydrolysis[2b] and can be easily derivatized,[3] which allowed their recent incorporation into nanostructured cathode materials based on carbon nanotubes[3a, 4] or dye-sensitized photocathode architectures.[5] While studies have been dedicated to understanding the tolerance to O_2[6] or the stability of this series of catalysts during H_2 evolution,[7] little information is available to benchmark their catalytic performances or to understand their catalytic mechanisms. Both complexes $[Co((DO)_2BF_2)pnBr_2]$ (**1**, Figure 1) and $[Co(DO)(DOH)pnBr_2]$ (**2**) ((DOH)(DOH)pn = $N^2,N^{2'}$-propanediylbis(2,3-butandione 2-imine 3-oxime) were previously reported as stable and efficient molecular catalysts for hydrogen evolution.[2b] However, at that time, the tools for a detailed mechanistic analysis obtained from information extracted from a thorough analysis of cyclic voltammograms (CVs) were not fully available. It is now the case thanks to the work of Prof. Jean-Michel Savéant to which this paper is dedicated.[8]

Herein we thus show that a combination of analysis of CVs in both total catalysis and canonical conditions, together with insights from theoretical calculations, allow us to propose a mechanism for the H_2 evolution reaction (HER) in organic solvent with **1** and **2** as molecular catalysts. We show that the H_2 formation step is kinetically important for both catalysts and that this step likely involves the ligand as a proton relay. In the case of **2** the oxime bridge in the tetradentate diimine-dioxime ligand is proposed to exist in two protonated states. The first protonation impacts the standard catalytic potential, but quantitative analysis show that this firstly added proton is not involved in catalysis due to a kinetically limiting reprotonation rate, contrasting here with the second protonation state.

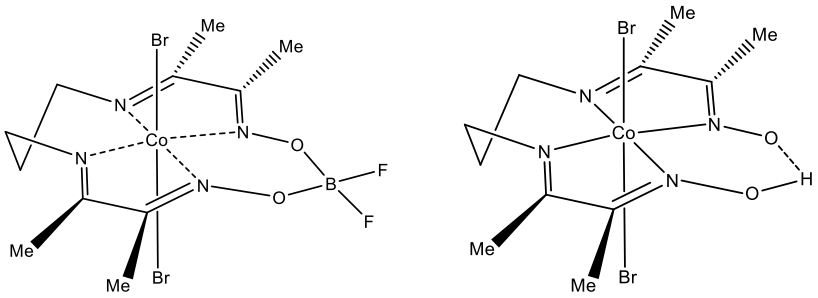

Figure 1. Structures of [Co((DO)$_2$BF$_2$)pnBr$_2$] (**1**, left) and [Co(DO)(DOH)pnBr$_2$] (**2**, right)

RESULTS AND DISCUSSION

Synthesis

Cobalt diimine-dioxime complexes **1** and **2** were synthesized using protocols optimized from the literature (see the supporting information). X-ray quality crystals of **1**·2/3 CH_2Cl_2 could be obtained from dichloromethane solution. The X-ray structure of **1** (Figure S5) reveals an octahedral environment around the cobalt ion with two axial halide ligands located *trans* to each other.

Cyclic Voltammetry

The cyclic voltammogram of **2** in CH_3CN (with 0.1 M *n*Bu_4NBF_4) displays two chemically reversible systems at –0.57 V (electrochemically quasi-reversible, ΔE_p = 169 mV) and –1.11 V (electrochemically reversible ΔE_p = 61 mV) vs Fc^+/Fc, corresponding to the $Co^{III/II}$ and $Co^{II/I}$ redox processes, respectively, based on previous literature.[2b] A third ligand-centered process is observed at –2.1 V (ΔE_p = 70 mV) vs Fc^+/Fc (Figure S6). From the peak current of the nernstian second redox event, $i_p = 0.446FSC_{cat}^0\sqrt{D_2Fv/RT}$, a diffusion coefficient D_2 of 1.4 10^{-5} $cm^2.s^{-1}$ is determined for **2**.[8f] C_{cat}^0 is the concentration of the complex, S is the electrode surface area, v is the scan rate, T is the temperature, F is the Faraday constant, and R is the gas constant. As previously noted, the presence of the $\{BF_2\}^+$ groups shifts all the redox processes ~200 mV

positively.[2b] The cyclic voltammogram of **1** in CH_3CN (with 0.1 M nBu_4NBF_4) also displays two chemically reversible systems at –0.38 V (electrochemically quasi-reversible ΔE_p = 142 mV) and –0.84 V (electrochemically reversible ΔE_p = 63 mV) vs Fc^+/Fc, corresponding to the $Co^{III/II}$ and $Co^{II/I}$ redox processes, respectively, based on previous literature.[2b] A third ligand-centered process is observed at –1.80 V (ΔE_p = 78 mV) vs Fc^+/Fc (Figure S6). A diffusion coefficient D_1 of 1.1 10^{-5} $cm^2.s^{-1}$ is determined for **1**.

Upon addition of *p*-cyanoanilinium tetrafluoroborate acting as a proton source, catalytic waves corresponding to H_2 evolution develop at potentials positive to the $Co^{II/I}$ wave as previously observed (Figure 2).[2b] In the case of **1** (Figure 2a), at slow scan rate (typically 0.1 V/s) and moderate substrate (*p*-cyanoanilinium) concentration, the situation is characteristic of a total catalysis regime,[8e, 8f] with the catalytic wave peaking because of limitation of the catalytic current by substrate diffusion due to its fast consumption in the diffusion-reaction layer. Catalysis is so fast that only a tiny amount of reduced catalyst is required to consume all the substrate in the diffusion-reaction layer; hence the catalytic peak is more positive than the standard potential of the catalyst, and this allows the $Co^{II/I}$ wave to be observed. As expected,[8f] the catalytic peak potential shifts cathodically with the acid concentration. As detailed later on, peak position in CV in the total catalysis regime can be used to extract kinetic information but it is not enough to fully characterize the reaction mechanism. Additional insights can be gathered from the regime encountered at large excess of substrate. The combination of fast kinetics (compared to the time scale of CV, i.e. pure kinetics conditions), and large excess of *p*-cyanoanilinium (compared to the catalyst) corresponds to the so-called canonical conditions where a steady-state S-shaped CV is expected.[8f] However, the observation of well-defined catalytic plateaus is often blurred by additional processes occurring at more negative potentials.[9] It may correspond to the reduction of substrate not consumed by the catalytic process of interest, be it another catalytic process involving a more reduced state of the molecular complex, direct proton reduction at the glassy carbon electrode, or proton reduction by catalytic materials formed at the electrode from the decomposition of the molecular catalyst.[7, 10] These side reactions thus require adaptation of the experimental conditions (substrate and catalyst concentrations and scan rate controlling the time scale of the CV).

For catalyst **1**, which was previously shown to be stable in the presence of *p*-cyanoanilinium tetrafluoroborate up to few tens of mM, figure 2b shows that, at 20 mM of acid and 1 mM of catalyst, raising the scan rate above 40 $V.s^{-1}$ leads to the observation of a current becoming independent of scan rate. Ohmic drop was carefully compensated so as to be confident in the shape of the rising part of the catalytic wave. It is clearly observed that the catalytic wave is not a simple S-shaped CV and that additional catalytic phenomena take place at potentials more negative than ca. –0.85 V vs Fc^+/Fc as attested by the change of the pace of the rising current. These phenomena are obviously not observed at small acid concentration due to acid consumption corresponding to total catalysis. From the experimental data, we estimate that a first pseudo-plateau current is obtained at roughly 0.9 mA for a catalyst concentration of 1 mM at a 1.6 mm diameter glassy carbon electrode. This is inferred from the observation of a scan rate independent inflexion zone in the catalytic wave. In the following we restrict our analysis to this first catalytic process (figure 2b). The additional current (above this pseudo-plateau) observed at high scan rate and high acid concentration is attributed to further reduction of the resting state intermediate triggering faster hydrogen evolution or possible catalysis mediated by electrode coatings originated from catalyst decomposition. At higher concentrations of acid (30 and 40 mM), it is seen (figure 2c) that the plateau current increases a bit but is not proportional to $\sqrt{[AH]}$. It is therefore a strong indication that the catalytic process becomes limited by a chemical step independent of acid concentration.

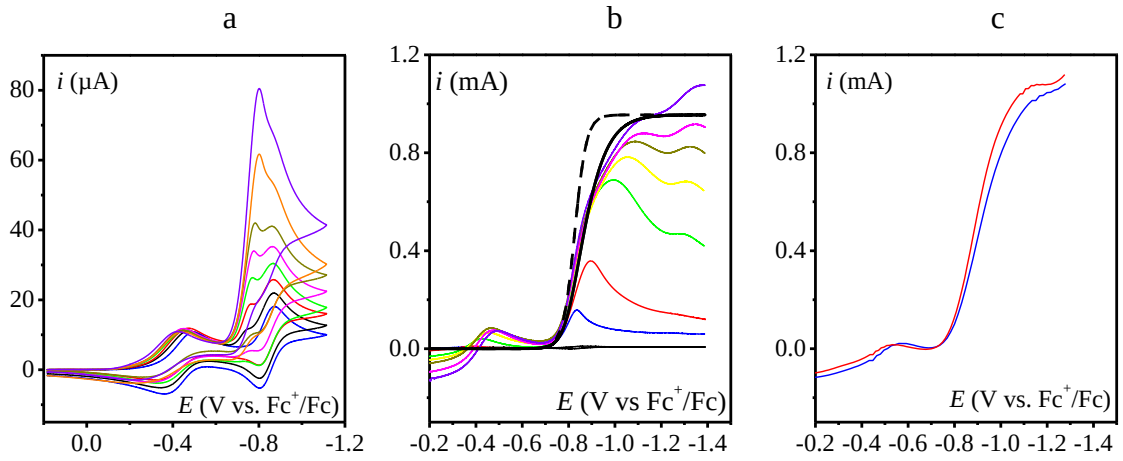

Figure 2. Cyclic voltammetry or linear sweep voltammetry (LSV) of H_2 evolution catalysis mediated by **1** in the presence of *p*-cyanoanilinium (AH) in CH_3CN + 0.1 M *n*-Bu_4NBF_4 on a 1.6

mm-diameter glassy carbon electrode. (a) [**1**] = 2 mM, v = 0.1 V.s^{-1}; [AH] = 0 (blue), 1 (black), 2 (red), 3 (green), 4 (magenta), 5 (dark yellow), 7.5 (orange), 10 (violet) mM. (b) [**1**] = 1 mM, [AH] = 0 mM and v = 0.1 V.s^{-1} (black); [AH] = 20 mM, v = 0.1 (blue), 1 (red), 10 (green), 20 (yellow), 30 (dark yellow), 40 (magenta), 60 (violet) V.s^{-1}. Thick full line: fitting with equation (4). Dashed thick line: fitting with equation (4) considering a nernstian electron transfer ($k_S \rightarrow \infty$), see text. (c) [**1**] = 1 mM, [AH] = 30 mM and v = 80 V.s^{-1} (blue); [AH] = 40 mM, and v = 60 V.s^{-1} (red). LSV have been translated vertically to get a zero current at the foot of the catalytic wave.

In the case of **2**, the behavior in the presence of *p*-cyanoanilinium tetrafluoroborate is strikingly different from **1** (Figure 3). At low concentration of acid (up to 4 mM), a peak shaped catalytic wave is observed, indicative of limitation by substrate diffusion, but the catalytic wave is so positively shifted (~350 mV) that it appears slightly negative to the $Co^{III/II}$ process (Figure 3a). It has been assigned to the protonation of the oximate function in the complex with opening of the oxime bridge.[2b, 11] A canonical behavior is observed with acid concentrations higher than 10 mM and scan rates in the 0.2-1 V.s^{-1} range (Figure 3b).

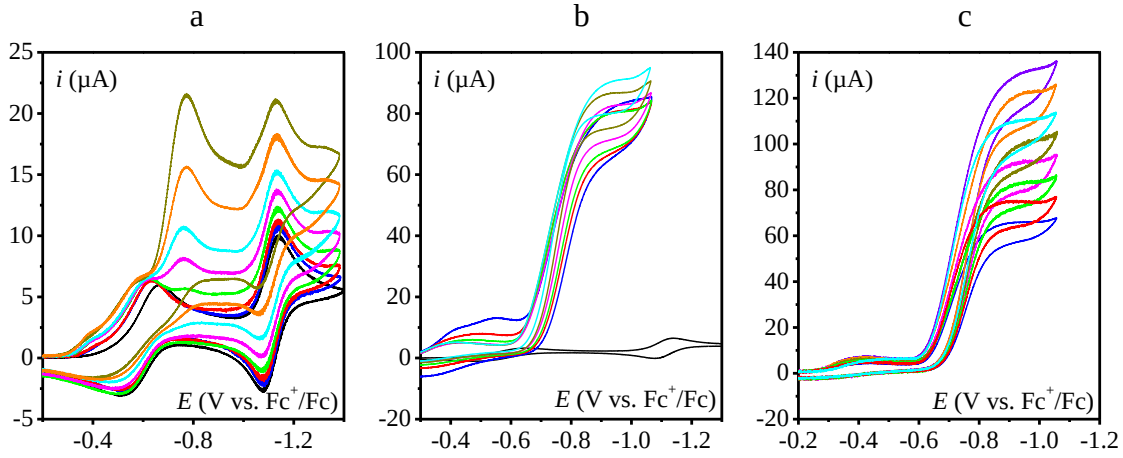

Figure 3. Cyclic voltammetry of H_2 evolution catalysis mediated by **2** in the presence of *p*-cyanoanilinium (AH) in CH_3CN + 0.1 M *n*-Bu_4NBF_4 on a 1.6 mm-diameter glassy carbon electrode. (a) [**2**] = 1 mM, v = 0.1 V.s^{-1}, [AH] = 0 (black), 0.25 (blue), 0.5 (red), 1 (green), 1.5 (magenta), 2 (cyan), 3 (orange), 4 (dark yellow) mM. (b) [**2**] = 0.5 mM; [AH] = 0 mM and v = 0.1 V.s^{-1} (black), [AH] = 10 mM and v = 1 V.s^{-1} (blue), [AH] = 15 mM and v = 0.5 V.s^{-1} (red); [AH] = 20 mM and v = 0.3 V.s^{-1} (green); [AH] = 25 mM and v = 0.2 V.s^{-1} (magenta); [AH] = 30

mM and v = 0.2 V.s^{-1} (dark yellow); [AH] = 35 mM and v = 0.2 V.s^{-1} (cyan). (c) [AH] = 20 mM, v = 0.2 V.s^{-1}and [**2**] = 0.5 (blue), 0.55 (red), 0.6 (green), 0.65 (magenta), 0.7 (dark yellow), 0.75 (cyan), 0.8 (orange), 0.85 (violet) mM.

Again, it is interesting to note that the plateau current does not depend on the concentration of acid below ~25 mM (Figure 3b). Above 25 mM of acid, the current slightly increases, which we could relate thanks to rinse test experiments[12] to the superimposition of a H_2 evolution catalytic process involving deposited cobalt particles.[7, 10] Discarding this process allows the determination of a maximal plateau current of 85 µA for a catalyst concentration of 0.5 mM and a 1.6 mm diameter glassy carbon electrode. We note that this plateau current is much smaller than the one obtained with catalyst **1** in similar conditions, indicating an intrinsically less efficient catalyst. The half-wave potential, $E_{pl,1/2}$, measured at the middle of the catalytic wave remains close to –0.73 V vs Fc^+/Fc for all the voltammograms recorded under canonical conditions (Figure 3b).

Mechanism for H_2 evolution catalyzed by **1** *and* **2**

Deciphering the mechanism of molecular catalysis of electrochemical reactions from CVs relies on the determination of reaction orders and identification of the kinetically determining steps. The mechanism for hydrogen production from acids electroreduction with molecular catalysts in an organic solvent has been studied extensively.[1, 13] In most cases, the mechanism involves a two-electron/two-step process starting with the reductive activation of the catalyst. A detailed analysis of various catalytic two-electron/two-step sequences was reported in 2014,[8a] in the framework of intermediates at steady-state and in canonical conditions and then in 2017 in the framework of total catalysis.[14] The analysis was later refined considering non-steady-state of intermediates.[15] Additional mechanisms involving bimolecular coupling have also been considered.[13a] However, none of the analyzed mechanisms correspond to a situation where the catalytic current is independent of the substrate (here acid) concentration, a feature observed for **1** and **2** and previously reported by Dempsey et al. for the parent $[Co(dmgBF_2)_2(CH_3CN)_2]$ catalyst (dmg^{2-} = dimethylglyoximato dianion).[16]

In addition, analytical treatment is unable to decipher between ECCE and ECEC catalytic pathways (E denotes a single electron transfer step and C a chemical step, here protonation) in the case where the second electron transfer occurs at a potential more positive than the first one for a reductive process as discussed here. An ECEC pathway starting from the Co^{II} state is nowadays accepted for cobaloximes.[17] The first EC sequence forms a Co^{III}-hydride species, which is then reduced at a potential more positive to that of the Co^{II}/Co^{I} couple to generate a Co^{II}-hydride intermediate. Protonation of the latter by the substrate (acid) forms H_2 and regenerates the starting Co^{II} state.

Regarding diimine-dioxime cobalt complexes, similar ECEC mechanisms have been postulated, namely based on DFT calculations of the catalytic cycle of **2** in 2013.[11] This study did however not encompass protonation of the diimine-dioxime ligand at the Co^{II} stage, which only can account for the large 350 mV shift of the catalytic wave with regards to the $Co^{II.}/Co^{I}$ couple. We therefore extended a previous study[18] in order to compute the standard potentials of the hydride couples $Co^{III}H/Co^{II}H$ for **1** and **2**. These calculations were calibrated on the standard potential of the Co^{II}/Co^{I} couple of **2**, and considered hexacoordinated Co^{II} or $Co^{III}H$, pentacoordinated (square pyramidal) Co^{I} and $Co^{II}H$ species (acetonitrile ligands are completing the indicated coordination sphere). Table 1 summarizes the standard potentials for the different couples under consideration. LH indicates protonation of the oxime bridge of the diimine-dioxime ligand.

Table 1. Experimental and calculated values of standard potentials.

E^0 (V vs Fc^+/Fc)	$E^0(Co^{II}/Co^{I})^{a,b}$	$E^0(Co^{II}LH/Co^{I}LH)^{a,b}$	$E^0(Co^{III}H/Co^{II}H)^{b}$	$E^0(Co^{III}HLH/Co^{II}HLH)^{b}$
1	–0.83 (–0.84)	–0.46	–0.68	*Not determined* [c]
2	–1.11 (–1.11)	–0.73	–1.05	–0.60[b]

a. Values from Table 1 of *ref. [18]*. Values in parentheses are experimental. Reference used was $E^0(Co^{II/I}) = -1.11$ V for **2**. Therefore, in the case of **2**, the calculated value matches experiment by construction.
b. Reduction accompanied by the loss of an axial ligand.
c. The protonation of the ligand is not relevant.

These calculations confirm that the hydride species $Co^{III}H$ are easier to reduce than the corresponding Co^{II} complex, thus indicating that ECEC pathways could be preferred. Such a sequence was thus considered for complex **1** with which catalysis takes place at the level of the Co^{II}/Co^{I} couple (figure 2). However, to account for the independence of the plateau current in

canonical conditions from acid concentration, we propose, as in the case of the parent $[Co(dmgBF_2)_2(CH_3CN)_2]$ catalyst, that an additional step is involved to close the catalytic loop corresponding to release of H_2. Therefore we introduce another intermediate in the catalytic cycle, namely $Co^{II}H,HL$ preceding H_2 release (scheme 1). At this stage, we do not speculate on the structure of this intermediate, i.e on the location of this additional proton.

Scheme 1. Proposed mechanisms for HER catalysed by **1**.

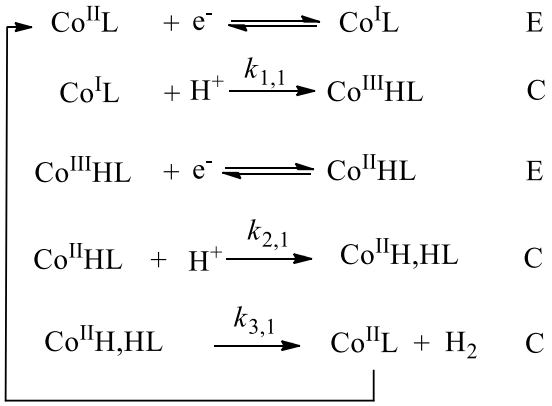

As for **2**, interestingly, the computed value[18] of the $Co^{II}LH/Co^{I}LH$ couple of **2** matches the observed mid-wave potential of catalysis in the canonical conditions. Therefore, in the case of **2**, it is reasonable to propose that protonation of the oxime bridge of the diimine-dioxime ligand occurs so that the catalysis is pinned at the potential of the $Co^{II}LH/Co^{I}LH$ couple. Protonation of the ligand can take place at the level of Co^{III} or Co^{II}, hence a square scheme is considered (Scheme 2). Once $Co^{I}LH$ is formed it can react with an acid molecule to form the hydride $Co^{III}HLH$ readily reduced according to the calculated standard potential (table 1). From $Co^{II}HLH$ two different pathways can be considered, depending on the role played by the proton initially installed on the ligand. If this proton on the ligand acts as a relay, H_2 is formed from an intramolecular proton transfer from the ligand to the hydride and then (or concertedly) released, leading to $Co^{II}L$.[11] This is then followed by reprotonation of the relay (Scheme 2, blue pathway). Alternatively, $Co^{II}HLH$ reacts with an exogenous acid molecule to form a doubly protonated species ($Co^{II}H,HLH$) from which H_2 is formed and released while the ligand remains protonated, hence regenerating $Co^{II}LH$ (Scheme 2, red pathway). Deciphering whether one or the other pathway is followed requires a quantitative kinetic analysis. Note that, as in the case of catalyst **1**

(scheme 1), at this stage, we do not speculate on the structure of the doubly protonated hydride, ($Co^{II}H$,HLH), i.e. the location of the third proton.

Scheme 2. Possible mechanisms for HER catalysed by **2**.

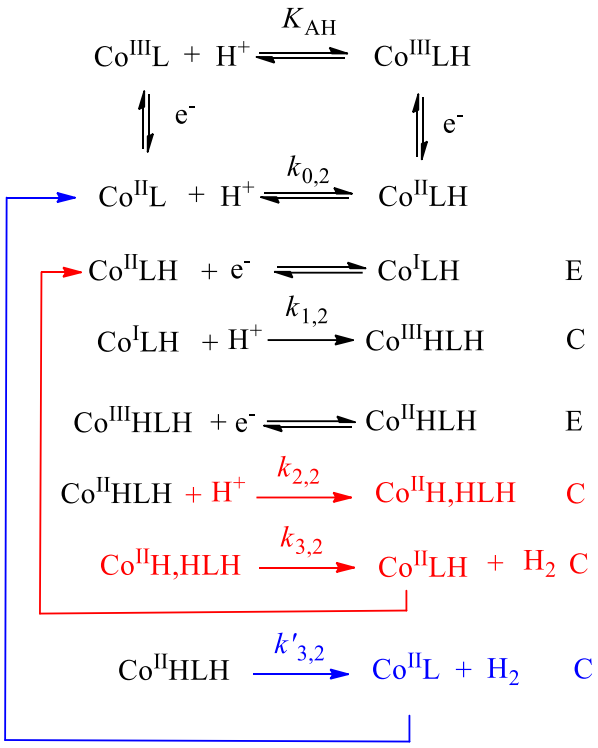

Quantitative analysis of the H_2 evolution mechanism

Considering the mechanistic framework depicted in schemes 1 and 2 and inferred from a combination of experimental observations, previous studies on cobaloxime-type catalysts and theoretical calculations, we propose a quantitative analysis of the catalytic processes. We first consider complex **1** whose behavior is similar to the previously studied parent [Co(dmgBF$_2$)$_2$(CH$_3$CN)$_2$] catalyst.[16] As shown in figure 2a, a total catalysis regime is observed at small concentration of acid, the peak current being proportional to acid concentration. From the catalytic *peak current*, the only information that can be retrieved is the substrate (*p*-cyanoanilinium) diffusion coefficient *D*, as $i_p = 0.609FSC^0_{AH}\sqrt{DFv/RT}$,[14] leading to $D = 1.2$ 10^5 cm^2 s^{-1}. Importantly, the peak current in total catalysis is independent from the catalyst characteristics. Kinetic information on catalysis can however be obtained from the *peak potential*. As shown in the Supporting Information (SI), total catalysis in the framework of an ECECC or

ECE'CC mechanism (where E' corresponds to the second electron transfer being homogeneous rather than at the electrode, i.e., $Co^{III}HL$ being reduced by $Co^{I}L$ with a second order rate constant k_e) leads to a peak potential E_p shifting cathodically by 30 mV per decade of scan rate, i.e. $\partial E_p / \partial \log v = -RT\ln 10/2F$. This is indeed observed experimentally (Figure S1), thus confirming the total catalysis regime. As justified a posteriori, we consider that the ECE'CC mechanism is dominant over the ECECC process in the experimental conditions of figure 2a, i.e. $k_e C^0_{cat} / k_{1,1} C^0_{\mathrm{AH}} >> 1$. It is thus shown (see SI) that the peak potential expression is:

$$E_p = E^0_{cat} - 0.409\frac{RT}{F} + \frac{RT}{2F}\ln\left(\frac{RT}{Fv}\frac{D_1}{D}\frac{2k_{1,1}C^{0\ 2}_{cat}}{C^0_{\mathrm{AH}}}\right) \qquad (1)$$

where E^0_{cat} is the standard potential of catalyst **1**. Taking the values determined for the diffusion coefficients and standard potential and the experimental values of the peak potential, we obtain that $k_{1,1}$ is on the order of 1.2 10^6 $M^{-1}s^{-1}$. Noting that the homogeneous reduction of $Co^{III}HL$ by $Co^{I}L$ is a downhill process, the corresponding rate constant k_e is assumed to be at the diffusion limit, i.e. $k_e \approx k_{dif} \approx 10^{10}$ $M^{-1}s^{-1}$, therefore the condition $k_e C^0_{cat} / k_{1,1} C^0_{\mathrm{AH}} >> 1$ is fulfilled. The observation that the plateau current at large concentration of acid and high rate constants becomes only slightly dependent on the substrate (acid) concentration indicates that the first chemical step (rate constant $k_{1,1}$) is not the rate determining step in canonical conditions. The expression of the plateau current in the framework of the ECE'CC mechanism is (see SI):

$$i_{pl} = \frac{FSC^0_{cat}\sqrt{D_1}}{\left[\begin{array}{l}\dfrac{1}{\sqrt{2k_{1,1}C^0_{\mathrm{AH}}}} - \dfrac{1}{\left(\sqrt{2k_{1,1}C^0_{\mathrm{AH}}}+\sqrt{k_{2,1}C^0_{\mathrm{AH}}}\right)}\dfrac{\sqrt{k_{1,1}}}{\sqrt{2k_{2,1}}}\left(\dfrac{k_{3,1}}{k_{2,1}C^0_{\mathrm{AH}}-k_{3,1}}\right) \\ + \dfrac{k_{2,1}C^0_{\mathrm{AH}} \times k_{1,1}C^0_{\mathrm{AH}}}{\left(k_{2,1}C^0_{\mathrm{AH}}-k_{3,1}\right)\left(\sqrt{2k_{1,1}C^0_{\mathrm{AH}}}+\sqrt{k_{3,1}}\right)\sqrt{2k_{1,1}C^0_{\mathrm{AH}}}\sqrt{k_{3,1}}}\end{array}\right]} \qquad (2)$$

We make the assumption that $k_{2,1}$ is larger than or of the same order of magnitude as $k_{1,1}$. This is in contrast to the parent $[Co(dmgBF_2)_2(CH_3CN)_2]$ catalyst, where the second proton transfer is slower than the first one.[16] However our assumption is underpinned by the observation that the half-wave potential is not significantly anodically shifted compared to the catalyst standard potential. At large acid concentrations, considering $k_{2,1}C^0_{AH} >> k_{3,1}$ and $k_{2,1} >> 2k_{1,1}$, equation (2) simplifies to:

$$i_{pl} = \frac{FSC^0_{cat}\sqrt{D_1}}{\left[\frac{1}{\sqrt{2k_{1,1}C^0_{AH}}} + \frac{\sqrt{k_{1,1}C^0_{AH}}}{\left(\sqrt{2k_{1,1}C^0_{AH}} + \sqrt{k_{3,1}}\right)\sqrt{2k_{3,1}}}\right]} \qquad (3)$$

Application of equation (3), taking the above determined values of $k_{1,1}$ and D_1, the plateau currents observed at 20, 30, 40 mM of acid (figure 3) lead to an evaluation of $k_{3,1} \approx 1.5\ 10^4\ s^{-1}$. Then, considering high scan rate corresponding to pure kinetics conditions and high enough acid concentrations so that the simplified equation is valid, the rising part of the CVs was simulated via equation (4), corresponding to the CV with possible interference of electron transfer kinetics described using the Butler-Volmer rate law (see SI):

$$i = \frac{i_{pl}}{1 + \frac{\exp\left[\frac{F}{RT}\left(E - E^0_{cat}\right)\right]}{1 + \frac{k_{1,1}C^0_{AH}}{\sqrt{2k_{1,1}C^0_{AH}k_{3,1}} + k_{3,1}}} + \frac{\sqrt{D_1}\exp\left[\alpha\frac{F}{RT}\left(E - E^0_{cat}\right)\right]}{k_{S,1}\left[\frac{1}{\sqrt{2k_{1,1}C^0_{AH}}} + \frac{k_{1,1}C^0_{AH}}{\sqrt{2k_{1,1}C^0_{AH}} + \sqrt{k_{3,1}}}\frac{1}{\sqrt{2k_{1,1}C^0_{AH}k_{3,1}}}\right]}} \qquad (4)$$

with $k_{S,1}$ being the standard rate constant for electron transfer for the $Co^{II}L/Co^{I}L$ couple, α being the transfer coefficient. We obtain a reasonable fitting of the experimental curve at high overpotential with equation (4) taking $k_{S,1}$ = 0.4 cm s^{-1} and α = 0.4, whereas a "fast" electron transfer cannot account for the rise of the current (figure 2b). We note that such a standard rate constant is large enough to ensure nernstian behavior of the $Co^{II}L/Co^{I}L$ couple at 0.1 V s^{-1} in the

absence of catalysis, as observed from the peak potential separation (63 mV); however, when catalysis is kinetically demanding electron transfer kinetics can interfere. In other words, it is important to recall that in canonical conditions, electron transfer kinetics is to be compared to the catalytic rate constant, here via the dimensionless parameter $\frac{k_{S,1}}{\sqrt{D_1}}\left[\frac{1}{\sqrt{2k_{1,1}C^0_{AH}}}+\frac{k_{1,1}C^0_{AH}}{\sqrt{2k_{1,1}C^0_{AH}}+\sqrt{k_{3,1}}}\frac{1}{\sqrt{2k_{1,1}C^0_{AH}k_{3,1}}}\right]$, whereas in the absence of catalysis it is compared to the diffusion rate constant via the dimensionless parameter $\frac{k_{S,1}}{\sqrt{Fv D_1/RT}}$. Thus, an apparently electrochemically fast (nernstian) catalyst in the absence of catalysis may not remain nernstian in catalytic conditions, in particular in pure kinetics conditions where $\frac{k_{1,1}C^0_{AH}}{Fv/RT} >> 1$ and $\frac{k_{3,1}}{Fv/RT} >> 1$. Finally, to test the consistency of our analysis, we performed digital simulations considering both the ECE'CC and ECECC mechanisms in parallel with the parameters determined so far (Figures S2 and S3). These simulations show that the trend of the increase of the catalytic current upon raising the scan rate and acid concentration observed experimentally is reproduced except for the additional current at potentials more negative than ca. –0.85 V vs Fc^+/Fc. This exception is attributed to faster catalysis due to further reduction of the resting state intermediate in the diffusion-reaction layer, i.e. $Co^{II}H,HL$ as $k_{3,1}$ becomes the dominant rate limiting constant. It was also confirmed that the value of $k_{2,1}$ has little or no influence on the CVs provided it is larger than $k_{1,1}$. A value of $k_{2,1}$ smaller than $k_{1,1}$ would lead to a smaller plateau current and a half wave potential more anodic than the catalyst standard potential. Hence our analysis is fully consistent.

We now consider catalyst **2**. Catalysis is triggered at a potential corresponding to the reduction of the bridge protonated ligand catalyst. Formation of $Co^{II}LH$ is obtained via the square scheme shown in Scheme 2. In the presence of a small amount of acid (up to 1 mM), we observe a small pre-wave at more positive potential than the $Co^{III}L/Co^{II}L$ wave and a small intensity for the $Co^{II}LH/Co^{I}LH$ wave. These observations rule out a kinetically fast protonation of $Co^{II}L$ (EC pathway) as it would imply an anodic shift of the whole one-electron $Co^{III}L/Co^{II}L$ process, and

the observation of a one-electron $Co^{II}LH/Co^{I}LH$ wave, of similar intensity as the $Co^{III}L/Co^{II}L$ wave, at ca. –0.73 V vs. Fc^{+}/Fc in the presence of one equivalent of acid (1mM). A small value of the rate constant for protonation of $Co^{II}L$ ($k_{0,2}$) has thus to be considered. This observation is surprising as one would have expected a fast protonation for such an O-H…O bridge. Simulations (see figure S4) show that the protonation rate constant has to be smaller than 200 M^{-1} s^{-1} to account for the small intensity of the $Co^{II}LH/Co^{I}LH$ wave in the presence of 1 mM of acid. From this upper value of the $k_{0,2}$ rate constant (200 $M^{-1}s^{-1}$) we can rule out the catalytic mechanism involving the ligand bridge acting as a proton relay (blue pathway in Scheme 2) as this step would prevent observation of a catalytic current as high as the one observed with 20 mM of acid (figure 3b). Indeed the maximal plateau current would be $i_{pl,\max} = FSC^{0}_{cat}\sqrt{D_2}\sqrt{2k_{0,2}C^{0}_{\mathrm{AH}}} \approx 18$ µA, which is much smaller than the experimental current ca. 85 µA. Moreover, if such an EC pathway is the only one at work to produce $Co^{II}LH$, no prewave is expected in front of the $Co^{III}L/Co^{II}L$ wave, contrary to the experimental observation. We are thus left with a CE process to form $Co^{II}LH$ and a catalytic mechanism with the ligand bridge not playing the role of a proton relay (red pathway in Scheme 2). The prewave observed in front of the $Co^{III}L/Co^{II}L$ is typical of a CE process kinetically limited by the chemical step or to a frozen equilibrium.[8f] From the observation that the intensity of the prewave at small acid concentration is comparable to the intensity of the $Co^{II}LH/Co^{I}LH$ wave, we posit a frozen (or very slow) equilibrium for protonation of the $Co^{III}L$. Therefore we can evaluate $E^{0}(Co^{III}LH/Co^{II}LH)$ to be ca. –0.4 V vs. Fc^{+}/Fc. Moreover for a 1mM:1mM catalyst:AH ratio, the relative intensities of the $Co^{III}LH$ reduction wave and of the $Co^{III}L$ reduction wave is roughly 0.3, indicating that the protonation equilibrium constant is ca. $K_{\mathrm{AH}} = 0.1$, keeping in mind that it is a bimolecular reaction in both directions with no conjugate base in the bulk. The effective concentration of $Co^{III}LH$, C^{eff}_{cat}, is obtained from $K_{\mathrm{AH}} = \dfrac{C^{eff\,2}_{cat}}{\left(C^{0}_{cat} - C^{eff}_{cat}\right)\left(C^{0}_{AH} - C^{eff}_{cat}\right)}$. We then note that, based on $K_{\mathrm{AH}} = 0.1$ and the standard potentials $E^{0}(Co^{III}LH/Co^{II}LH)$ = -0.4 V vs. Fc^{+}/Fc and $E^{0}(Co^{III}L/Co^{II}L)$ = -0.57 V vs. Fc^{+}/Fc, we can evaluate the equilibrium constant for protonation of the oxime bridge on $Co^{II}L$ to be roughly 10^{2}. This slightly favourable protonation step has a

forward rate constant estimated above to be below 200 $M^{-1}s^{-1}$. Hence the unfavourable protonation of the oxime bridge on $Co^{III}L$ can be estimated to be slow enough for the equilibrium to be frozen on the time scale of CV. Protonation of the oxime bridge is associated with breaking of this bridge. This might be the reason why the reaction is so slow. In the presence of 0.5 mM catalyst and 10 to 30 mM acid (conditions of figure 3b), the effective concentration of the actual catalyst $Co^{III}LH$, C_{cat}^{eff}, can be calculated to be ranging from 0.37 to 0.46 mM. Taking the data reported in figure 3b, we find that the plateau current is approximately proportional to this effective concentration (Figure 4a). Then in the framework of the mechanism depicted in scheme 2 (red pathway), considering that the second electron transfer is homogeneous and that the acid concentration independent step is the rate determining step (as the plateau current is independent of the acid concentration), we have $i_{pl} = 2FSC_{cat}^{eff}\sqrt{D_2}\sqrt{k_{3,2}}$ from which we obtain $k_{3,2} \approx 220$ s^{-1} noting that the plateau current is actually proportional to C_{cat}^{eff} as expected for a heterolytic mechanism. Taking the set of data corresponding to figure 3c, we obtain $k_{3,2} \approx 160$ s^{-1} (Figure 4b). Given the approximations made in the analysis, we can estimate this determination to be reasonable. Extraction of kinetic data other than from the plateau current is not possible given that we do not know the standard potential with accuracy. Moreover $k_{3,2}$ is small enough for this step to be rate determining at relatively low acid concentration, making kinetic control by other steps ($k_{1,2}$ and $k_{2,2}$) difficult to observe.

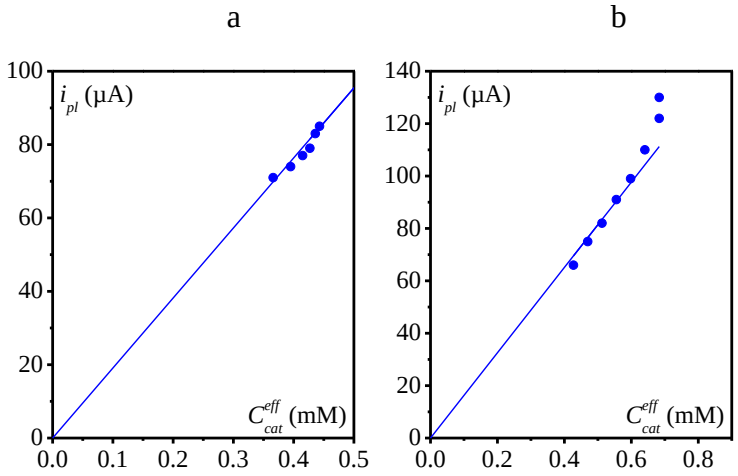

Figure 4. Catalytic plateau currents as functions of the effective concentration of the actual catalyst resulting from protonation of **2**, C_{cat}^{eff}. (a) Data from CVs shown in figure 3b. (b) Data from CVs shown in figure 3c.

Benchmarking and discussion

From our quantitative analysis, we observe that both catalysts **1** and **2** reach a maximal turnover frequency independent of acid concentration: $TOF_{\max,1} = k_{3,1}$ and $TOF_{\max,2} = k_{3,2}$.[8a] This maximal turnover frequency is roughly one order of magnitude larger with **1** compared to **2**, but the latter has a catalytic standard potential 110 mV more positive than the former. This is summarized in the catalytic Tafel plots (CTP) represented in figure 5 for both **1** and **2** together with the parent $[Co(dmgBF_2)_2(CH_3CN)_2]$ whose standard potential is $E^0(Co^{II}/Co^{I})$ = –0.914 V vs. Fc^+/Fc.[16, 19] CTPs represent the turnover frequency (*TOF*) as function of the overpotential $\eta = E^0_{\text{target}} - E$ where E^0_{target} is the standard potential of the target reaction, i.e. 2 AH + 2 e = 2 A^- + H_2 (AH is *p*-cyanoanilinium). Based on previous evaluation taking into account homoconjugation and standard state for AH, we have E^0_{target} = –0.47 V vs Fc^+/Fc. [20] For the sake of simplicity and with the aim to get a rough comparison of the catalysts, CTPs have been drawn assuming a hypothetical large concentration of acid, 1 M, so that maximal turnover frequencies are independent of acid concentration for all three catalysts. In such a framework and considering an ECE'CC mechanism, it can be shown (see SI) that the expression of *TOF* is:

$$TOF_i = \frac{k_{3i}}{1+\sqrt{\frac{2k_{3i}}{k_{1i}C^0_{\text{AH}}}}\exp\left(\frac{F\left(-\eta+\left(E^0_{\text{target}}-E^0_i\right)\right)}{RT}\right)+\frac{2\sqrt{D_{cat,i}k_{3i}}}{k_{S,i}}\exp\left(\frac{\alpha F\left(-\eta+\left(E^0_{\text{target}}-E^0_i\right)\right)}{RT}\right)}$$

To plot CTPs in Figure 5, we used the determined $k_{S,1}$ value, resulting in a rounded shape as previously described in another context.[21] We made the assumption that $k_{S,i}$ is large enough for catalyst **2** and the parent $[Co(dmgBF_2)_2(CH_3CN)_2]$ to prevent interference of electron transfer kinetics. k_1 was determined to be 2.0 10^8 M^{-1} s^{-1} for the parent $[Co(dmgBF_2)_2(CH_3CN)_2]$.[16] $k_{1,2}$

could not be evaluated from CV analysis, but we make the favorable assumption that it is of the same order of magnitude as $k_{1,1}$, hence 10^6 M^{-1} s^{-1}.

It is seen that catalysts **1** and **2** surpass the parent [Co(dmgBF$_2$)$_2$(CH$_3$CN)$_2$] both in term of maximal activity but also for activity at low overpotential. Catalyst **1** is definitively the more efficient at large overpotential. At low overpotential catalyst **2** is more efficient than catalyst **1** due to protonation of the oxime bridge lowering the standard potential of the actual catalyst. However, catalyst **2** is surpassed as the overpotential is increased.

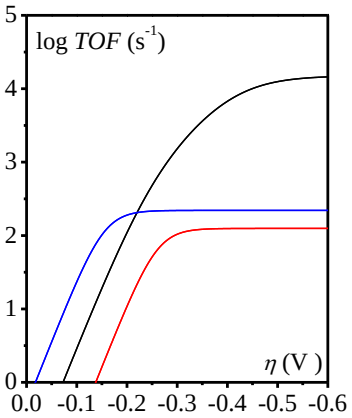

Figure 5. Catalytic Tafel plots. log*TOF* as a function of the overpotential in conditions of large excess of substrate (*p*-cyanoanilinium, 1 M) for catalyst **1** (black), **2** (blue) and [Co(dmgBF$_2$)$_2$(CH$_3$CN)$_2$] (red).

Finally, our results raise a question regarding the actual meaning of the step characterized by the rate constant $k_{3,i}$ and consequently on the possible role of the ligand as an acid/base functionality. Several mechanisms can be envisioned. A simple release of H_2 sitting on the cobalt was proposed in the case of the parent [Co(dmgBF$_2$)$_2$(CH$_3$CN)$_2$] catalyst, in which case the corresponding rate constant was evaluated as 125 s^{-1},[16] Although possible, simple H_2 release is not very likely because the rate constant is changing by one order of magnitude by modification of the ligand. Alternatively, we can propose that this rate constant corresponds to a step involving formation of H_2 via an intramolecular proton transfer from the ligand to the hydride. This implies that the preceding step is a protonation of the ligand, either the oxime oxygen (Scheme 3) or the nitrogen. We note that both protonation of the oxime oxygen or nitrogen is probably thermodynamically unfavorable,[19] preventing a definitive conclusion. Importantly, in the case of

catalyst **2**, as shown above, the involved proton for H_2 formation is not the first one protonating the oxime bridge. This avoids a mechanistic pathway where a slow protonation of the relay would limit the overall rate. Indeed, as recently emphasized by J-M. Savéant, the boosting effect of a proton relay requires a proper relay, i.e., insuring fast protonation and re-protonation during the catalytic cycle.[22]

It appears from our analysis and our mechanistic proposition that the intramolecular proton transfer from the protonated oxime to the hydride to form H_2 is much more efficient in catalyst **1** compared to catalyst **2** and the parent $[Co(dmgBF_2)_2(CH_3CN)_2]$. The rationale behind this observation has yet to be elucidated, but our data show that fine tuning of the ligand can drastically modify intrinsic reactivity.

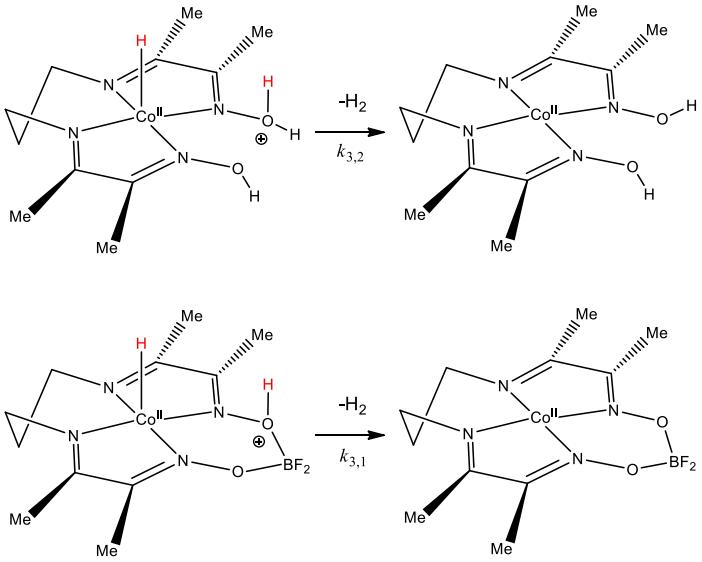

Scheme 3. Proposed mechanism for H_2 formation step.

CONCLUSION

This comprehensive analysis of the catalytic mechanism for H_2 evolution mediated by cobalt diimine-dioxime catalysts confirms an ECEC-type pathway going through a Co(II)-hydride intermediate, as previously documented for the parent cobaloximes. If the first protonation step is metal-centered, the second proton is possibly relayed by a basic site present on the ligand, likely an oxygen or nitrogen atom of the oxime function. “En passant”, we document the first case of a basic site with a proper pKa value installed on the ligand but unable to act as a proton relay

because of slow reprotonation rate.[22] Turnover frequency of cobalt diimine-dioxime catalysts is finally controlled by H_2 release which can be proposed to be an intramolecular coupling between the hydride ligand and the protonated ligand, leading to a catalytic rate that is independent of proton concentration in the canonical regime. As saturation of the catalytic current with increasing proton concentration has already been observed[23] yet not fully analyzed except in the case of the [Co(dmgBF$_2$)$_2$(CH$_3$CN)$_2$] catalyst,[16] this feature is likely quite general amongst catalysts with proton relays.[24] The methodology presented here will allow more comprehensive analyses to fill this gap in the future.

Supporting Information.

Experimental details. Derivation of equations. Details on theoretical calculations. Digital simulations. Crystal data information.

Notes

The authors declare no competing financial interest.

Acknowledgments

This work was supported by the European Research Council and European Commission's Seventh Framework Program (FP7/2007-2013) under grant agreement n° 306398 (project Photocat**H**$_2$ode) and the French National Research Agency (Labex ARCANE, CBH-EUR-GS, ANR-17-EURE-0003). The theory portion of this work was supported by the Center for Molecular Electrocatalysis, an Energy Frontier Research Center, funded by the U.S. Department of Energy, Office of Science, Basic Energy Sciences.

References

[1] V. Artero, J.-M. Saveant, *Energy Environ. Sci.* **2014**, *7*, 3808-3814.

[2] a) N. Kaeffer, M. Chavarot-Kerlidou, V. Artero, *Acc. Chem. Res.* **2015**, *48*, 1286–1295; b) P.-A. Jacques, V. Artero, J. Pécaut, M. Fontecave, *Proc. Natl. Acad. Sci. U.S.A.* **2009**, *106*, 20627-20632.

[3] a) E. S. Andreiadis, P. A. Jacques, P. D. Tran, A. Leyris, M. Chavarot-Kerlidou, B. Jousselme, M. Matheron, J. Pecaut, S. Palacin, M. Fontecave, V. Artero, *Nat. Chem.* **2013**, *5*, 48-53; b) N. Queyriaux, E. S. Andreiadis, S. Torelli, J. Pecaut, B. S. Veldkamp, E. A. Margulies, M. R. Wasielewski, M. Chavarot-Kerlidou, V. Artero, *Faraday Discuss.* **2017**, *198*, 251-261.

[4] N. Coutard, N. Kaeffer, V. Artero, *Chem. Commun.* **2016**, *52*, 13728-13748.
[5] a) N. Kaeffer, J. Massin, C. Lebrun, O. Renault, M. Chavarot-Kerlidou, V. Artero, *J. Am. Chem. Soc.* **2016**, *138*, 12308-12311; b) N. Kaeffer, C. D. Windle, R. Brisse, C. Gablin, D. Léonard, B. Jousselme, M. Chavarot-Kerlidou, V. Artero, *Chem. Sci.* **2018**, *9*, 6721–6738; c) C. D. Windle, J. Massin, M. Chavarot-Kerlidou, V. Artero, *Dalton Trans.* **2018**, *47*, 10509-10516; d) S. Bold, J. Massin, E. Giannoudis, M. Koepf, V. Artero, B. Dietzek, M. Chavarot-Kerlidou, *ACS Catal.* **2021**, *11*, 3662-3678; e) Y. Chen, H. Chen, H. Tian, *Chem. Commun.* **2015**, *51*, 11508-11511.
[6] N. Kaeffer, A. Morozan, V. Artero, *J. Phys. Chem. B* **2015**, *119*, 13707-13713.
[7] N. Kaeffer, A. Morozan, J. Fize, E. Martinez, L. Guetaz, V. Artero, *ACS Catal.* **2016**, *6*, 3727-3737.
[8] a) C. Costentin, J.-M. Savéant, *ChemElectroChem* **2014**, *1*, 1226-1236; b) J.-M. Savéant, E. Vianello, *Advances in Polarography; 1 ed., Vol. 1*, Pergamon Press, Cambridge, U. K., **1959**; c) J. M. Saveant, K. B. Su, *J. Electroanal. Chem.* **1984**, *171*, 341-349; d) J. M. Savéant, *Elements of Molecular and Biomolecular Electrochemistry*, Wiley, **2006**; e) J. M. Saveant, *Chem. Rev.* **2008**, *108*, 2348-2378; f) J. M. Savéant, C. Costentin, *Elements of Molecular and Biomolecular Electrochemistry, 2nd Ed.*, John Wiley & Sons, Hoboken, NJ, **2019**.
[9] C. Costentin, S. Drouet, M. Robert, J.-M. Savéant, *J. Am. Chem. Soc.* **2012**, *134*, 11235-11242.
[10] S. Cobo, J. Heidkamp, P.-A. Jacques, J. Fize, V. Fourmond, L. Guetaz, B. Jousselme, V. Ivanova, H. Dau, S. Palacin, M. Fontecave, V. Artero, *Nat. Mater.* **2012**, *11*, 802-807.
[11] A. Bhattacharjee, E. S. Andreiadis, M. Chavarot-Kerlidou, M. Fontecave, M. J. Field, V. Artero, *Chem. Eur. J.* **2013**, *19*, 15166-15174.
[12] V. Artero, M. Fontecave, *Chem. Soc. Rev.* **2013**, *42*, 2338-2356.
[13] a) C. Costentin, H. Dridi, J.-M. Savéant, *J. Am. Chem. Soc.* **2014**, *136*, 13727-13734; b) C. G. Margarit, N. G. Asimow, A. Thorarinsdottir, C. Costentin, D. G. Nocera, *ACS Catal.* **2021**, *11*; c) T. Straistari, R. Hardre, J. Fize, S. Shova, M. Giorgi, M. Reglier, V. Artero, M. Orio, *Chem. Eur. J.* **2018**, *24*, 8779.
[14] C. Costentin, D. G. Nocera, C. N. Brodsky, *Proc. Natl. Acad. Sci. USA* **2017**, *114*, 11303-11308.
[15] C. Costentin, J. M. Saveant, *ACS Catal.* **2018**, *8*, 5286-5297.
[16] E. S. Rountree, D. J. Martin, B. D. McCarthy, J. L. Dempsey, *ACS Catal.* **2016**, *6*, 3326-3335.
[17] V. Artero, M. Chavarot-Kerlidou, M. Fontecave, *Angew. Chem. Int. Ed.* **2011**, *50*, 7238-7266.
[18] B. H. Solis, Y. Yu, S. Hammes-Schiffer, *Inorg. Chem.* **2013**, *52*, 6994-6999.
[19] a) C. Baffert, V. Artero, M. Fontecave, *Inorg. Chem.* **2007**, *46*, 1817-1824; b) X. L. Hu, B. M. Cossairt, B. S. Brunschwig, N. S. Lewis, J. C. Peters, *Chem. Commun.* **2005**, *41*, 4723-4725.
[20] V. Fourmond, P. A. Jacques, M. Fontecave, V. Artero, *Inorg. Chem.* **2010**, *49*, 10338-10347.
[21] C. Costentin, M. Robert, J.-M. Savéant, A. Tatin, *Proc. Natl. Acad. Sci. USA* **2015**, *112*, 6882-6886.
[22] J. M. Saveant, *Angew. Chem. Int. Ed.* **2019**, *58*, 2125-2128.
[23] a) U. J. Kilgore, J. A. S. Roberts, D. H. Pool, A. M. Appel, M. P. Stewart, M. R. DuBois, W. G. Dougherty, W. S. Kassel, R. M. Bullock, D. L. DuBois, *J. Am. Chem. Soc.* **2011**,

133, 5861-5872; b) A. M. Appel, D. L. DuBois, M. R. DuBois, *J. Am. Chem. Soc.* **2005**, *127*, 12717-12726.
[24] Z. Thammavongsy, I. P. Mercer, J. Y. Yang, *Chem. Commun.* **2019**, *55*, 10342-10358.